Aerospace Science and Technology 77 (2018) 585–594

Contents lists available at ScienceDirect

Aerospace Science and Technology

www.elsevier.com/locate/aescte

Tube-based robust model predictive control for spacecraft proximity operations in the presence of persistent disturbance

M. Mammarella [a,*], E. Capello [b], H. Park [c], G. Guglieri [a], M. Romano [d]

[a] Department of Mechanical and Aerospace Engineering, Politecnico di Torino, Corso Duca degli Abruzzi 24, 10129, Torino, Italy
[b] Department of Mechanical and Aerospace Engineering, CNR-IEIIT, Politecnico di Torino, Corso Duca degli Abruzzi 24, 10129, Torino, Italy
[c] Department of Mechanical and Aerospace Engineering, New Mexico State University, Las Cruces, NM, USA
[d] Department of Mechanical and Aerospace Engineering, Naval Postgraduate School, 1 University Circle, Monterey, CA 93943, USA

ARTICLE INFO

Article history:
Received 17 November 2017
Received in revised form 9 March 2018
Accepted 5 April 2018
Available online 9 April 2018

Keywords:
Robust control
Model predictive control
Automated rendezvous and docking

ABSTRACT

Rendezvous and Proximity Operations (RPOs) of two autonomous spacecraft have been extensively studied in the past years, taking into account both the strict requirements in terms of spacecraft dynamics variations and the limitations due to the actuation system. In this paper, two different Model Predictive Control (MPC) schemes have been considered to control the spacecraft during the final phase of the rendezvous maneuver in order to ensure mission constraints satisfaction for any modeled disturbance affecting the system. Classical MPC suitably balances stability and computational effort required for online implementation whereas Tube-based Robust MPC represents an appealing strategy to handle disturbances while ensuring robustness. For the robust scheme, the computational effort reduction is ensured adopting a time-varying control law where the feedback gain matrix is evaluated offline, applying a Linear Matrix Inequality approach to the state feedback stabilization criterion. An extensive verification campaign for the performance evaluation and comparison in terms of constraint satisfaction, fuel consumption and computational cost, i.e. CPU time, has been carried out on both a three degrees-of-freedom (DoF) orbital simulator and an experimental testbed composed by two Floating Spacecraft Simulators reproducing a quasi-frictionless motion. Main conclusions are drawn with respect to the mission expectations.

1. Introduction

Automated rendezvous and docking (RVD) missions have been widely studied in the last ten years. During these missions, controlled trajectories, in which a Chaser spacecraft tries to reach and dock a Target spacecraft, are guaranteed by a control system, able to handle uncertainties and external environment disturbances. Different control techniques have been proposed in literature, including feedback-linearization-based approach [1], Riccati equation techniques [2], sliding-mode control (SMC) [3], and other control setups in [4,5]. In [1] the problem of motion synchronization of free-flying robotic spacecraft and serviceable floating objects in space is considered, but a limitation of this approach is that the linear system can be different from the nonlinear one, due to the cancellation of nonlinearities. The Riccati equation techniques (as in [2]) are simple, numerically stable and competitive in computational effort with other known methods. However, only small parametric uncertainties are included. In [3] SMC strategies are proposed for thruster control, even if it is deemed to lead to excessive fuel consumption, due to switching on/off thrusters at high frequency. Even if a fuel-efficient algorithm is proposed, a high consumption is verified to track the docking port. As clearly explained in [4], a model predictive control approach for spacecraft proximity maneuvering which could effectively handle the constraints on thrust magnitude, line-of-sight, and approach velocity, and can be more effective than other controllers in terms of fuel consumption.

For this reason, in this research, special attention has been reserved to the adoption of MPC, for its ability to deal with the constraints that typically characterize this maneuver, both in terms of relative position and velocity, as well as actuation system limitations. The approach proposed here moves along the lines of previous works employing MPC schemes for RVD. A Linear Quadratic MPC (LQMPC) has been adopted to enforce thrust magnitude limitation, line of sight (LOS) constraints, and velocity constraints for soft docking in [6]. In [7], a low-complexity MPC scheme for three degree-of-freedom (DoF) spacecraft system is developed for the low-thrust rendezvous and proximity operations.

However, in all of these approaches, orbital perturbations, disturbances, and model errors are not taken into account. In [8],

* Corresponding author.
E-mail addresses: martina.mammarella@polito.it (M. Mammarella), hjpark@nmsu.edu (H. Park).

https://doi.org/10.1016/j.ast.2018.04.009
1270-9638/

the improved performance of a robust MPC in the presence of disturbances, compared with a classical one, are highlighted solving the spacecraft rendezvous problem. In the last years, focusing on robust approach, a new appealing approach has been introduced, called Tube-based Robust MPC (TRMPC), which focuses on two main goals: (i) the robustness to additive disturbances and (ii) the computational efficiency of a classical MPC. Moreover, this algorithm is split in two parts: (i) an offline evaluation of the constraints to ensure the uncertain future trajectories lie in sequence of sets, known as *tubes*, and (ii) the online MPC scheme applied to the nominal trajectories, representing the center of the tube itself as in [9].

The main ideas of this paper are to evaluate the performance of a robust MPC controller, both in simulations and on an experimental setup, and to demonstrate the real-time effectiveness of the proposed robust approach. Moreover, this proposed MPC controller is able to handle uncertainties due to external disturbances and additive noise, according to the recent trend in literature [10]. Starting from the approach proposed in [11], our idea is to evaluate for the first time the performance of this controller within the space rendezvous scenario both in simulation, for a three degree-of-freedom (DoF) orbital simulator, and in an experimental setup, i.e. in a three DoF air-bearing spacecraft testbed. Hence, a real-time implementation of the TRMPC approach is here proposed to test the effectiveness of the controller on board.

In order to reach a reasonable computational effort for the robust approach, a time-varying control law is adopted where the feedback gain matrix is evaluated offline. A Linear Matrix Inequalities (LMI) approach is applied to the state feedback stabilization criterion for the stability analysis and the evaluation of the feedback matrix. As explained in [12] and in [13], the proposed method improves the computational efficiency of a robust MPC even using low-thrust propulsion, typically adopted in the final phase of RVD maneuver, as in the proposed case-study. Furthermore, due to the presence of parametric physical uncertainties and discrepancies between the mathematical model and the actual dynamics of the physical system in operation, as non linearities and neglected high-order dynamics, the LMI approach is able to reduce the computational effort required by other robust controller, guaranteeing the stability of the system and improving real-time implementation feasibility. The modeled uncertainties are related to the model linearization of the Hill–Clohessy–Wiltshire (HCW) equations, in which the coupling between the position and speed variables and the quadratic terms related to the distance between the Target and the chaser are neglected. In detail, all the terms $o(\rho^2/R^2)$ are not considered, with ρ the distance between the two spacecraft and R the distance between the Target and the Earth [14]. Moreover, the uncertainties of the control matrix are related to the mass and inertia variation due to the fuel consumption. The LMI approach applied to the Edge Theorem, generalization of the Kharitonov Theorem, allows the offline definition of the feedback gain matrix, which is adopted to define the time-varying control law. Further information of both Edge Theorem and Kharitonov Theorem can be found in [16]. Finally, the robust TRMPC is compared with a classical LQMPC in terms of computational cost, fuel consumption, and constraints satisfaction when the system is affected by persistent bounded uncertainties. The LQMPC, proposed in this paper, was deeply validated in [15], in which a LQMPC and inverse dynamics in the virtual domain (IDVD) guidance methods are combined.

An extensive verification campaign, both in simulation and in an experimental testbed, has been accomplished to validate the performance of the TRMPC. Its compatibility for real-time implementation and constraint satisfaction has been verified when the system is affected by bounded additive disturbances. As said before, the simulations are carried out on a three DoF orbital simulator. Instead, the experimental verification has been carried out using two spacecraft that float over a polished granite monolith surface reproducing a quasi-frictionless motion in Spacecraft Robotics Laboratory at the Naval Postgraduate School [17].

The paper is organized as follows. In Section 2 and 3 the model setup, both of the simulation environment (three DoF) and of the experimental testbed are presented. The control objective and the system dynamics are explained in detail in Section 4. In Section 5 the MPC design is described, focusing on the theory of the TRMPC and how the concept of Tube is introduced and defined, according to a constraint tightening approach. The simulation results obtained with the three DoF orbital simulator are presented in Section 6 while experimental results are described in Section 7, together with a comparison of the performance of LQMPC and TRMPC. Main conclusions are drawn in Section 8.

Notation: The notation employed is standard. Blackboard boldface letters (e.g., $\mathbb{X}$) denote sets. Bold letters, e.g., $\mathbf{u}_k = [u_{0|k} \cdots u_{N-1|k}]$, are used to denote the stack vector of N predicted values. Positive (semi)definite matrices $\boldsymbol{A}$ are denoted as $\boldsymbol{A} \succ 0$ ($\boldsymbol{A} \succeq 0$), whereas negative (semi)definite matrices are denoted as $\boldsymbol{A} \prec 0$ ($\boldsymbol{A} \preceq 0$). The set $\mathbb{I}_{\geq 0}$ denotes the positive integers, including 0. We use x_k for the (measured) state at time k and $\mathrm{x}_{i|k}$ for the state predicted i steps ahead at time k. $A \oplus B$ and $A \ominus B$ denotes the Minkowski sum and Pontryagin set difference, respectively.

2. Model of the translational three DoF relative orbital maneuver

The nominal relative motion of the two spacecraft in neighboring orbits can be described through HCW linearized equations in the typical continuous-time state-space formulation as $\dot{\mathrm{x}} = \boldsymbol{A}\mathrm{x} + \boldsymbol{B}\mathrm{u}$, where $\mathrm{x} = [x, y, z, \dot{x}, \dot{y}, \dot{z}]$ is the state vector representing the 3-position and 3-velocity components of the Chaser with respect to the Target in the local coordinate system (Local Vertical Local Horizontal (LVLH) frame), $\mathrm{u} = [F_x, F_y, F_z]$ is the control vector, expressed in the body reference frame, represented by the control force components applied to the spacecraft through the actuation system. As described in [18], the LVLH coordinate system is centered on the center of mass (CoM) of the Target and the axes are defined as follows: the X axis (V_{bar}) is in the direction of the orbital velocity vector, the Y axis (H_{bar}) is in the opposite direction of the angular momentum vector of the orbit, while the Z axis (R_{bar}) is radial from the spacecraft center of mass to the CoM Earth. The Chaser has the goal to arrive in the proximity of the Target vehicle, considering a V-bar approach within a cone corridor. $\boldsymbol{A}$ and $\boldsymbol{B}$, the state and control matrices respectively, are defined as in [19] as a function of the angular velocity of the orbit (known and constant) with respect to the inertial frame ω_0 and the wet mass of the Chaser m_{CV}.

Due to the space environment, external disturbances in terms of forces and moments, such as the J2, the gravity gradient, and the solar radiation pressure, could affect the vehicle performance and drive the chaser to violate the constraints. If these additive noises are included in the spacecraft dynamics, the following continuous-time uncertain system shall be considered

$$\dot{\mathrm{x}} = \boldsymbol{A}\mathrm{x} + \boldsymbol{B}\mathrm{u} + \boldsymbol{B}_w\mathrm{w}, \tag{1}$$

where w is the vector of persistent noise, mainly related to the external environment and can be modeled as a random and bounded noise. In particular, the disturbance sequence is the realization of a stochastic process where $\mathrm{w} \in \mathbb{W}$ is a random variable with known distribution, and the set $\mathbb{W}$ is a compact and convex set, containing the origin in its interior. Then, a discrete-time representation of system (1) is derived as follows

$$\mathrm{x}_{k+1} = \boldsymbol{A}_d\mathrm{x}_k + \boldsymbol{B}_d\mathrm{u}_k + \boldsymbol{B}_{w_d}\mathrm{w}_k, \tag{2}$$

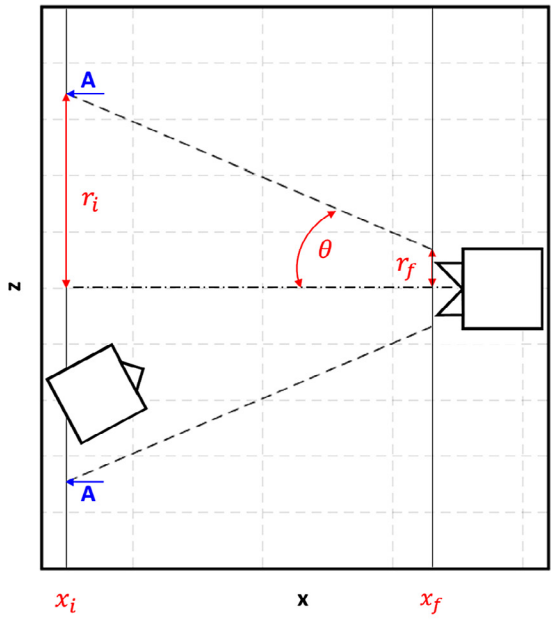

(a) $x-z$ orbital plane

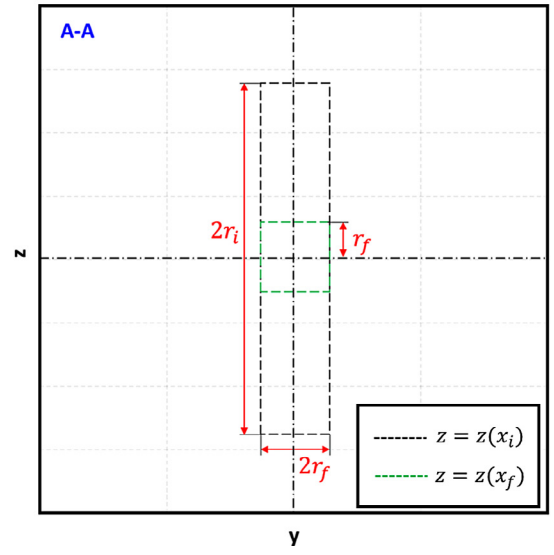

(b) $y-z$ normal-to-orbit plane

Fig. 1. Cone approach for 3DoF Orbital Simulator. (For interpretation of the colors in the figure(s), the reader is referred to the web version of this article.)

where $\boldsymbol{A}_d, \boldsymbol{B}_d$, and $\boldsymbol{B}_{w_d}$ are the discrete matrices corresponding to the continuous ones in (1). A goal of the control is to drive the system to the docking position, compliant with the constraints satisfaction in terms of position and velocity during the proximity maneuver. In a typical cone-approach maneuver (see Fig. 1), the Chaser should lie within the projection of the approach cone in the $x-z$ orbital plane. As shown in Fig. 1(a), the Chaser starts the rendezvous maneuver at $x = x_i$ and ends up to $x = x_f$, where the docking phase begins. The angle θ defines the approaching truncated cone and is a function of the cone bases radius, i.e. the initial one r_i and r_f. In Fig. 1(b), the constraints in the $y-z$ plane are represented with respect to the section $A-A$ identified in Fig. 1(a). As we can notice, the constraint set for the position along y is fixed and equal to $[y_{min}, y_{max}] = [-r_f, r_f]$ whereas, in compliance with Fig. 1(a), the constraints along z are time-varying, since the radius of the cone decreases from r_i at $z = z(x_i)$ (black dashed rectangle) to r_f at $z = z(x_f)$ (green dashed rectangle).

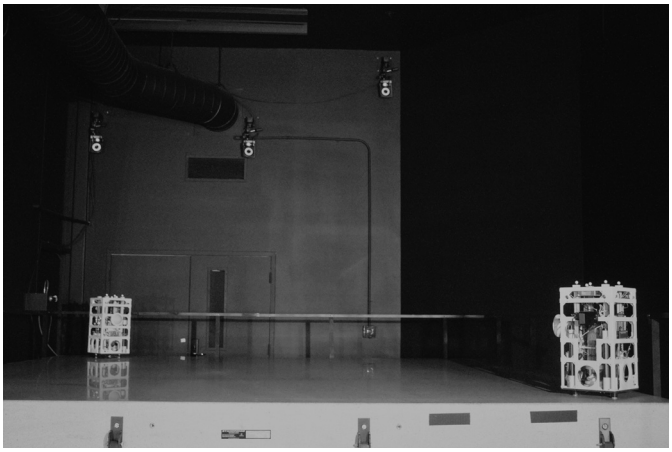

Fig. 2. NPS-POSEIDYN testbed with the Vicon motion capture cameras, FSSs, and granite monolith in the Spacecraft Robotics Laboratory at the Naval Postgraduate School. The Target FSS is on the right and the Chaser FSS is on the left.

The related position boundaries can be expressed as follows

$$x_i \leq x \leq x_f,$$
$$-r_f \leq y \leq r_f,$$
$$|z| \leq (x_f - x)\tan\theta - (r_i - r_f),$$

whereas the velocity constraints are defined in order to bound each velocity components norm to be less or equal to the maximum one, defined for the maneuver. Hard constraints are considered also on the input, in order to be compliant with the saturation of the actuation system. The input constraint set is defined according to the maximum level of thrust that the actuators can provide.

3. Model of the planar experimental testbed

The two controllers, the TRMPC as well as the LQMPC for comparison reasons, are experimentally tested on the Naval Postgraduate School (NPS) Proximity Operation of Spacecraft: Experimental hardware-In-the-loop DYNamic simulator (POSEIDYN) testbed. The NPS-POSEIDYN testbed consists of Floating Spacecraft Simulators (FSS), a polished granite monolith, a Vicon motion capture system, and a ground station computer. Fig. 2 shows an overview of the testbed.

The floating surface is a 15 ton, 4-by-4 meter granite monolith, with a planar accuracy of ± 0.0127 mm and a horizontal leveling accuracy of less than 0.01 deg. The FSSs float over the granite surface via three flat air bearings. The quasi-frictionless environment with the low residual acceleration of the FSS emulates the environment in space. The FSS has eight cold gas thrusters fed by compressed air from an on-board tank [20]. Using the on-board computer the FSS is able to perform real-time computation of guidance and control algorithms. The Vicon motion capture system, composed of ten overhead cameras that track reflectors mounted on the FSS, provides accurate position and orientation data. These data are streamed to the FSS using a Wi-Fi connection. They are then augmented with angular velocity measurements provided by an on-board fiber-optic gyroscope. A discrete Kalman filter processes the data and provides a full state estimate. Detailed description of the NPS-POSEIDYN testbed can be found in [17].

The FSS dynamic model consists of three double integrators, two translational and one rotational DoF. The discrete-time dynamics in the presence of additive disturbances is described in a state-space formulation as (1), with the discrete-time state, control, and disturbance matrices corresponding to the continuous ones reported below

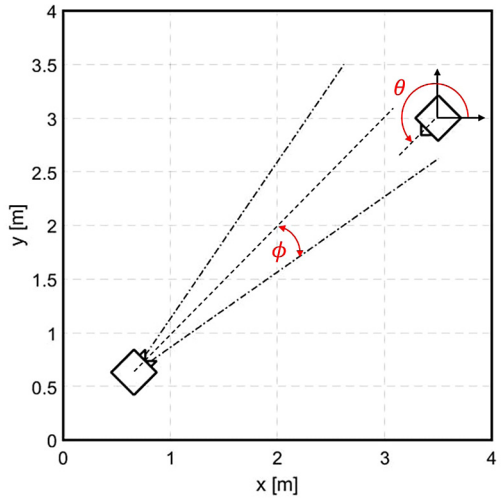

Fig. 3. Cone approach for 3DoF NPS-POSEIDYN testbed.

$$\boldsymbol{A} = \begin{bmatrix} 0_{3\times3} & \mathbb{I}_3 \\ 0_{3\times3} & 0_{3\times3} \end{bmatrix}, \quad \boldsymbol{B} = \begin{bmatrix} & 0_{3\times3} & \\ \frac{1}{m} & 0 & 0 \\ 0 & \frac{1}{m} & 0 \\ 0 & 0 & \frac{1}{I_z} \end{bmatrix}, \quad \boldsymbol{B}_w = \mathbb{I}_6, \tag{3}$$

where m and I_z are the mass and moment of inertia about the vertical axis of the FSS, respectively.

The Chaser FSS is constrained to lie within a cone (see Fig. 3) and the related boundaries are translated in position constraints as

$$x_T \leq x \leq x_T + x_i\sqrt{2}\cos(\frac{\pi}{4} \pm \phi)/\cos\phi,$$

$$y_T \leq y \leq y_T + x_i\sqrt{2}\sin(\frac{\pi}{4} \pm \phi)/\cos\phi,$$

where ϕ is the cone angle and (x_T, y_T) are the final position of the FSS Chaser, corresponding to the FSS Target position. Bounded constraints are also introduced for the velocity components and the relative attitude, as described in Section 5.

The polytope set for the additive disturbance has to be defined. Hence, the persistent uncertainty has been evaluated first through simulations, and then the results have been validated experimentally with respect to the testbed environment. According to the specifications of the cold gas thrusters, a random error related to the thrust magnitude has been taken into account, considering a ±10% error over the maximum thrust level available. Then, the same mission profile has been simulated two times. First, both the external environment and the actuation system have been considered ideal, i.e., not affected by disturbance. Next, the simulation has been repeated considering noise from the environment and random error affecting the thrusters. Hence, the states evolutions have been compared, in order to size the maximum disturbance level that can affect the system. Then, these results have been later validated with the characterization of the testbed, performing several experiments, considering same initial conditions.

4. System dynamics and control objective

Let consider a generic model of the form (2), where the noise is a realization of a stochastic process, each one an independent and identically distributed (i.i.d.), zero-mean random variable, with bounded and convex support $\mathbb{W} \in \mathbb{R}^n$, containing the origin in its interior.

The system is subject to hard constraints on both the state and input of the form

$$\mathrm{x} \in \mathbb{X}, \quad \mathrm{u} \in \mathbb{U}, \tag{4}$$

where $\mathbb{X}$ and $\mathbb{U}$ are polytope.

To solve the control problem, a robust MPC algorithm is considered [11], repeatedly solving the following optimal control problem where the finite horizon quadratic cost $J_N(\mathrm{x}, \mathbf{u})$ to be minimized at the current time k is

$$J_N(\mathrm{x}_k, \mathbf{u}_k) = \sum_{i=0}^{N-1} (\mathrm{x}_{i|k}^T \boldsymbol{Q}\, \mathrm{x}_{i|k} + \mathrm{u}_{i|k}^T \boldsymbol{R} \mathrm{u}_{i|k}) + \mathrm{x}_{N|k}^T \boldsymbol{P} \mathrm{x}_{N|k}, \tag{5}$$

where $\boldsymbol{Q} \in \mathbb{R}^{n\times n}$, $\boldsymbol{Q} \succ 0$, $\boldsymbol{R} \in \mathbb{R}^{m\times m}$, $\boldsymbol{R} \succ 0$, and $\boldsymbol{P}$ is the solution of the discrete algebraic Riccati equation.

Due to the presence of a bounded and persistent unknown disturbance w, the state of the system

$$\mathrm{x}_{i|k} = \mathrm{z}_{i|k} + \mathrm{e}_{i|k} \tag{6}$$

can be split into a nominal part, $\mathrm{z}_{i|k}$, and an error part, $\mathrm{e}_{i|k}$, which represents the deviation of the actual state $\mathrm{x}_{i|k}$ with respect to the nominal one. Applying the following feedback policy

$$\mathrm{u}_{i|k} = \mathrm{v}_{i|k} + \boldsymbol{K}(\mathrm{x}_{i|k} - \mathrm{z}_{i|k}), \tag{7}$$

where the matrix $\boldsymbol{K}$ is chosen so that $\boldsymbol{A}_K = \boldsymbol{A} + \boldsymbol{B}\boldsymbol{K}$ is Schur stable, then the corresponding nominal and error dynamics can be described respectively by

$$\mathrm{z}_{i+1|k} = \boldsymbol{A}\mathrm{z}_{i|k} + \boldsymbol{B}\mathrm{v}_{i|k}, \quad \mathrm{z}_{0|k} = \mathrm{x}_{0|k}, \tag{8}$$

$$\mathrm{e}_{i+1|k} = \boldsymbol{A}_K \mathrm{e}_{i|k} + \boldsymbol{B}_w \mathrm{w}_{i|k}, \quad \mathrm{e}_{0|k} = 0. \tag{9}$$

Hence, the finite horizon optimal quadratic cost (5) can be redefined in terms of nominal state z_k and control input $\mathbf{v}_k$ as

$$J_N(\mathrm{z}_k, \mathbf{v}_k) = \sum_{i=0}^{N-1} (\mathrm{z}_{i|k}^T \boldsymbol{Q}\, \mathrm{z}_{i|k} + \mathrm{v}_{i|k}^T \boldsymbol{R} \mathrm{v}_{i|k}) + \mathrm{z}_{N|k}^T \boldsymbol{P} \mathrm{z}_{N|k}, \tag{10}$$

and the related finite horizon optimal control problem can be reformulated as follows.

Definition 1 *(Nominal finite horizon optimal control problem).* Given the nominal system dynamics (8), cost (10) and nominal constraints set $\mathbb{Z}$, $\mathbb{V}$, and $\mathbb{Z}_f$, the nominal Robust MPC finite horizon optimization problem is

$$\min_{\mathbf{v}} J_N(\mathrm{z}_k, \mathbf{v}_k) \tag{11a}$$

$$\begin{aligned} \text{s.t.} & \mathrm{z}_{i+1|k} = \boldsymbol{A}\mathrm{z}_{i|k} + \boldsymbol{B}\mathrm{v}_{i|k}, \quad \mathrm{z}_{0|k} = \mathrm{x}_k, \\ & \mathrm{z}_{i|k} \in \mathbb{Z}, \quad i \in [1, N], \\ & \mathrm{v}_{i|k} \in \mathbb{V}, \quad i \in [0, N-1], \\ & \mathrm{z}_{N|k} \in \mathbb{Z}_f. \end{aligned} \tag{11b}$$

The solution of (11) is the optimal nominal control sequence $\mathbf{v}_{0|k}^*(\mathrm{z}_k) = [v_{0|k}^*(0; \mathrm{z}_k), \cdots, v_{T-1|k}^*(T-1; \mathrm{z}_k)]$ and the first control action, i.e., $\tilde{\kappa}_N(\mathrm{z}_k) := v_{0|k}^*(0; \mathrm{z}_k)$, represents the optimal control to be applied. The correspondent control applied on the uncertain system, according to the control policy adopted, is

$$\kappa_N(\mathrm{x}_k, \mathrm{z}_k) = \tilde{\kappa}_N(\mathrm{z}_k) + \boldsymbol{K}(\mathrm{x}_k - \mathrm{z}_k). \tag{12}$$

The composite close-loop system then satisfies

$$\begin{aligned} \mathrm{x}_{i+1|k} &= \boldsymbol{A}\mathrm{x}_{i|k} + \boldsymbol{B}\kappa_N(i, \mathrm{x}_k, \mathrm{z}_k) + \boldsymbol{B}_w \mathrm{w}_{i|k}, \\ z_{i+1|k} &= \boldsymbol{A}\mathrm{z}_{i|k} + \boldsymbol{B}\tilde{\kappa}_N(i, \mathrm{z}_k). \end{aligned} \tag{13}$$

For the TRMPC approach, considering discrete-time Linear Time Invariant (LTI) formulation of the system and the control policy defined in Eq. (7), the $\boldsymbol{K}$ matrix is defined to stabilize the system. The stability analysis has been performed considering the application of the LMI approach to the state feedback stabilization criterion, applying the definition of Schur stability to the closed-loop system

$$\mathrm{x}_{i+1|k} = (\boldsymbol{A} + \boldsymbol{BK})\mathrm{x}_{i|k} + \boldsymbol{B}\mathrm{v}_{i|k} + \boldsymbol{B}_w \mathrm{w}_{i|k}, \tag{14}$$

Hence, the satisfaction of the following condition aims to define the feedback gain matrix $\boldsymbol{K}$ that stabilize the system

$$(\boldsymbol{A} + \boldsymbol{BK})^T \hat{\boldsymbol{P}}(\boldsymbol{A} + \boldsymbol{BK}) - \hat{\boldsymbol{P}} \prec 0, \quad \hat{\boldsymbol{P}} \succ 0. \tag{15}$$

Adopting a feedback linearization control strategy implies the definition of a state feedback control law able to overcome system nonlinearities and, at the same time, to impose some desired linear dynamics. On the other hand, the control scheme success is strongly dependent on how much the model description of the system under consideration fit with the real physical system in operation. Hence, linearizing the system dynamics means introducing in the plant parametric uncertainties representing the discrepancies between the mathematical model and the actual dynamics, in terms of neglected nonlinearities, unmodeled high-frequency dynamics, and deliberate reduced-order models. Furthermore, additional parametric uncertainties are represented by system-parameters variations due to environmental and/or physical changes. All these errors introduced in the model have to be considered since they might affect the performance as well as the stability of the control system. Therefor, a stability analysis must be performed in which parametric uncertainties related to the application studied are explicitly considered. In this work, the stability analysis has been evaluated through an LMI approach applied to the well-known Edge Theorem, which is an extension of Karitonov's theorem ([16]) and states that the stability of a polytope of polynomials can be guaranteed by the stability of its one-dimensional exposed edge polynomials [21]. The Edge Theorem takes into account the dependence of the polynomial coefficients on the uncertain parameters and the coefficients of the polynomials are affine functions of the uncertain vector $q = [q_1, ..., q_l]$, bounded in the hyper-rectangle B_q defined by

$$B_q := \left\{ q \in \mathbb{R}^l \mid q_i \in [q_i^-, q_i^+], i = 1, ..., l \right\}. \tag{16}$$

Theorem 1 *(Edge Theorem). Consider the polytope of polynomials $\tilde{P}$, defined as*

$$\tilde{P} = \Big\{ p(s,q) = a_0(q) + a_1(q)s + ... + a_{n-1}(q)s^{n-1} + s^n : a_i(q) = a_{i_0} + \sum_{k=1}^{l} a_{i_k} q_k, q \in B_q, \quad i = 0, ..., n-1 \Big\}. \tag{17}$$

The family $\tilde{P}$ is Hurwitz if and only if all edges of $\tilde{P}$ are Hurwitz (see [22]). Starting from the discrete nominal state and control matrices, $\boldsymbol{A}_d$ and $\boldsymbol{B}_d$, the corresponding uncertain matrices are defined as $\boldsymbol{A}_d^- = \boldsymbol{A}_d(q-)$, $\boldsymbol{A}_d^+ = \boldsymbol{A}_d(q+)$, $\boldsymbol{B}_d^- = \boldsymbol{B}_d(q-)$, and $\boldsymbol{B}_d^+ = \boldsymbol{B}_d(q+)$.

Then, a system of four LMI is defined to solve a joint stabilization problem based on the Edge Theorem and Lyapunov stability condition, coupling the uncertain matrices defined before. The feedback matrix $\boldsymbol{K}$, used to define a time-varying control law, is derived through this approach and ensures the stability of the system for every modeled uncertainty that may affect the system itself.

In this work, the adopted linearized dynamics of the Chaser spacecraft relative to the Target vehicle during the final approach of the rendezvous maneuver has been derived by Clohessy and Wiltshire in [14], starting from the nonlinear equations for the restricted three-body problem and considering for the both the spacecraft a reference circular orbit around a master body. Considering the two spacecraft mass infinitesimal with respect to the mass of the main body and defining $\rho = \rho \mathrm{i}_\rho$ and $\mathrm{r}_1 = r_1 \mathrm{i}_\xi$ as the position vectors of the Chaser and the Target spacecraft respectively, and with $\mathrm{r} = r\,\mathrm{i}_\xi$ the vectorial sum of the two positions, $\mathrm{r} = \rho + \mathrm{r}_1$, the equations of motion of the Chaser spacecraft can be rewritten as

$$\frac{d^2\rho}{dt^2} + 2\omega \times \frac{d\rho}{dt} + \omega \times [\omega \times (\rho + \mathrm{r}_1)] = -\frac{\omega^2 r_1^3}{r^3}\mathrm{r}, \tag{18}$$

where ω is the orbital angular rate. This differential equation presents nonlinearities due to the term $1/r^3$. As described in [14], the use of a Taylor Series expansion allows to obtain a linear equation if we ignore the higher order terms, i.e. $\mathrm{O}(\rho^2/r_1^2)$ as $\frac{r_1^3}{r^3} = 1 - 3\,\mathrm{i}_\xi \cdot \mathrm{i}_\rho \frac{\rho}{r_1} + \mathrm{O}(\frac{\rho^2}{r_1^2})$. Then, Eq. (18) reduces to

$$\frac{d^2\rho}{dt^2} + 2\omega \times \frac{d\rho}{dt} + \omega \times (\omega \times \rho) = -\omega^2\rho + 3\omega^2(\mathrm{i}_\xi \cdot \rho)\mathrm{i}_\xi + \mathrm{O}(\rho^2). \tag{19}$$

We finally get the linearized differential equation for the motion of the Chaser relative to the Target spacecraft as

$$\frac{d^2\rho}{dt^2} + 2\omega \times \frac{d\rho}{dt} = -\omega^2\zeta\,\mathrm{i}_\zeta + 3\omega^2\xi(\mathrm{i}_\xi + \mathrm{O}(\rho^2). \tag{20}$$

Ignoring the $\mathrm{O}(\rho^2)$ and expressing the position vector in a more convenient way as

$$\rho \equiv \mathrm{r} = x\,\mathrm{i}_\theta + z\,\mathrm{i}_r - y\,\mathrm{i}_y, \;\; \mathrm{i}_{r_1} = \mathrm{i}_r \;\; \omega = -\omega\,\mathrm{i}_y, \tag{21}$$

with x in the direction of the motion i_θ, z in the radial direction i_r and $\mathrm{i}_y = \mathrm{i}_\theta \times \mathrm{i}_r$ normal to the orbital plane. Then, we can obtain the scalar form of Eq. (19), which is the well-known HCW Equation. Hence, the parametric uncertainty introduced in the model are of the same order of $\mathrm{O}(\rho^2/r_1^2)$ and $\mathrm{O}(\rho^2)$. When external forces are acting on the system, in this case due to the correction actions actuated by the thrusters (F_x, F_y, F_z) of the AOCS subsystem, we have

$$\begin{aligned} \frac{d^2x}{dt^2} - 2\omega\frac{dz}{dt} &= \frac{F_x}{m_{CV}}, \\ \frac{d^2y}{dt^2} + \omega^2 y &= \frac{F_y}{m_{CV}}, \\ \frac{d^2z}{dt^2} + 2\omega\frac{dx}{dt} - 3\omega^2 z &= \frac{F_z}{m_{CV}}. \end{aligned} \tag{22}$$

Therefore, additional uncertainties have been introduced in terms of minimal physical changes of the Chaser spacecraft mass m_{CV} during the maneuver as well as environmental impact on the orbital angular velocity ω. Furthermore, for what concern the experimental setup, additional simplifications have been introduced, since the Chaser FSS dynamics is represented by only three double integrators, ignoring the coupling between the two translational DoFs and the angular velocity, and the inertia with respect to the axis normal to the motion is considered for the rotational dynamics, implying new physical uncertainties. All these errors have been taken into account for the stability analysis and the evaluation of the feedback gain matrix, which has been derived offline, reducing the computational effort usually required to robust controllers and allowing the real-time implementation.

5. Tube-based robust MPC approach

5.1. Definition of tube-based approach

In order to robustly satisfy the mission constraints, they are tightened to allow the trajectories of the uncertain system, affected by disturbance, to lie in a tube centered on the nominal one, where each trajectory is related to a particular realization of the uncertainty at each time step k. In this Section, the derivation of the nominal state, input, and terminal constraints set $\mathbb{Z}$, $\mathbb{V}$, and $\mathbb{Z}_f$ are described according to the approach proposed in [11], so that the constraints (4) of the system (2) are satisfied for every realization of the disturbance sequence $\mathbf{w}$, by suitable design of the tube.

Let define $S_K(\infty) := \sum_{j=0}^{\infty} \boldsymbol{A}_K^j \mathbb{W}$, the uncertain set of the error $\mathrm{e}_{i|k}$, as the minimal robust positive invariant set for $\mathrm{x}_{i+1|k} = \boldsymbol{A}\mathrm{x}_{i|k} + \boldsymbol{B}_w \mathrm{w}_{i|k}$, $\mathrm{w} \in \mathbb{W}$. Then, the state and control constraints are satisfied if

$$\begin{aligned} &\mathrm{z}_{i|k} \in \mathbb{X} \ominus S_K(\infty), \\ &\mathrm{v}_{i|k} \in \mathbb{U} \ominus \boldsymbol{K} S_K(\infty). \end{aligned} \tag{23}$$

Satisfaction of the terminal constraint at time instant N for the uncertain system (2) is ensured if the nominal system satisfies the *tighter* constraint

$$\mathrm{z}_N \in \mathbb{Z}_f \subseteq \mathbb{X}_f - S_K(\infty), \quad \mathbb{Z}_f \subseteq \mathbb{Z}. \tag{24}$$

These assertions only make sense if the disturbance set $\mathbb{W}$ is sufficiently small to satisfy the following Assumption 1, as defined in [11].

Assumption 1 *(Restricted disturbances for constraints satisfaction).* $S_K \subset \mathbb{X}$ and $\boldsymbol{K} S_K \subset \mathbb{U}$.

The next step consists in the definition of a robust positively invariant set S_K for (9) to obtain the tighter constraints acting on the nominal system. Then the constraints are considered for the TRMPC problem. Several methods can be adopted, as proposed in [23], [24], and [25]. Once the uncertainty set $\mathbb{W}$ is evaluated, an inner approximation of the nominal constraint set is defined, according to the following strategy presented in [11]:

1. Consider a single linear constraint as
$$\mathbb{X} = \left\{ \mathrm{x}_{i|k} \in \mathbb{R}^n \mid a\mathrm{x}_{i|k} \leq b \right\}.$$
2. Since $\mathrm{x}_{i|k} = \mathrm{z}_{i|k} + \mathrm{e}_{i|k}$ for all $i \in \mathbb{I}_{\geq 0}$, where $\mathrm{e}_{i|k} \in S_K(\infty)$, it follows that
$$a\mathrm{z}_{i|k} \leq b - \max\left\{ a\mathrm{e}_{i|k} \mid \mathrm{e}_{i|k} \in S_K(\infty) \right\} = b - \Phi_\infty.$$
3. Compute an upper approximation of Φ_∞ as
$$\Phi_N = \max\left\{ a \textstyle\sum_{i=0}^{N-1} \boldsymbol{A}_K^i \mathrm{w}_{i|k} \mid \mathrm{w}_{i|k} \in \mathbb{W} \right\}.$$
4. Considering the feedback control matrix $\boldsymbol{K}$ and the prediction horizon N, $\boldsymbol{A}_K^N \in \alpha\mathbb{W}$ with $\alpha \in (0, 1)$. We then obtain
$$\Phi_\infty \leq (1-\alpha)^{-1}\Phi_N.$$
5. Hence, the constraint set $\mathbb{Z}$ can be defined as
$$\mathbb{Z} := \left\{ \mathrm{z}_{i|k} \in \mathbb{R}^n \mid a\mathrm{z}_{i|k} \leq b - (1-\alpha)^{-1}\Phi_N \right\}.$$

Analogous procedure has been used to obtain a suitable control constraint set $\mathbb{V}$.

Algorithm 1 Constraint tightening.

```
procedure CONSTRAINT TIGHTENING
    Define 𝕏, 𝕌, and 𝕎
    Set α ∈ (0, 1)
    Evaluate N subject to A_K^N ∈ α𝕎
    Compute Φ_N
    Evaluate ℤ, 𝕍 and ℤ_f
end procedure
```

Algorithm 2 Feedback gain evaluation.

```
procedure
    Define B_q as in (16)
    Build (A_i, B_i)_{q∈supp(B_q)}
    for each i-th vertex (A^i, B^i) do
        Build (A_i, B_i)_{q∈supp(B_q)}
        sys_i = X A_i^T + A_i^T X − Y^T B_i^T − B_i^T Y
    end for
    Solve [X ≻ 0, sys_i ≺ 0]
    Get X and Y
    Get K = Y X^{-1}
end procedure
```

Algorithm 3 TRMPC algorithm.

```
procedure
    Set N
    At current time k for i = 0, evaluate x_{i=0|k} = x_k
    for i = 0 : N − 1 do
        Set z_{i=0|k} = z_0 = x_k
        Solve (11)
    end for
    Get v_0(z_0)
    Get v_0(0; z_0) and evaluate z_{k+1} applying v_0(0; z_0) on Eq. (8)
    Evaluate u_k according to Eq. (7), then evaluate x_{k+1} applying u_k on Eq. (2)
end procedure
```

5.2. Tube-based robust MPC algorithm

Once the tube is defined in order to contain all the trajectories of an uncertain system subject to additive disturbances, an optimal control problem can be formulated. The solution of the problem provides a control policy that minimizes a quadratic cost. The solution also ensures that the state and control constraints are satisfied for all admissible bounded disturbance sequences. The application of TRMPC guarantees that the trajectory evolved from the initial state lies within a robust positive invariant set, defined to satisfy state and control constraints acting on the system, allowing to control the uncertain system (2) by constraining its trajectory to lie within a tube whose center is the solution of the nominal system (8) obtained applying the implicit MPC control law $\tilde{\kappa}_N(\mathrm{z}_k)$. The final TRMPC algorithm can be divided into two parts: (i) an offline computation of the feedback matrix $\boldsymbol{K}$, which stabilizes the system (described in detail in Section 4), and of the tightened constraints set $\mathbb{Z}$ and $\mathbb{V}$, as shown in Algorithm 1 and Algorithm 2, and (ii) the repeated online optimization problem, i.e., Algorithms 3.

6. Simulation results

The LQMPC approach has been already validated in a simulation environment, as described in [6], where it has been shown how this approach can effectively handle various constraints arising in rendezvous and proximity operations in the orbital plane. ESA's ORCSAT project [26] has investigated the adoption of LQMPC on the Mars Sampling Return capture scenario. Moreover, LQMPC has already been tested in space by PRISMA project to demonstrate Guidance, Navigation, and Control (GNC) strategies for spacecraft formation flying and rendezvous, considering a classical MPC control for fuel saving based on orbit propagation [27]. On the other hand, these studies do not consider the robustness of the controller to persisting disturbances due to several sources that can strongly

Table 1
Cone geometry and mission scenario definition.

Parameter	Value
x_i	350 [m]
x_f	0 [m]
r_i	7 [m]
r_f	0.1 [m]
θ	10 [deg]

Table 2
3DoF state and control tightened constraints.

Parameter	Nominal system value
F_{max}	$[-0.99, 0.99]$ [N]
(x_{min}, x_{max})	$[-349.97, 4.97]$ [m]
(z_{min}, z_{max})	$[-6.97, 6.97]$ [m]
(y_{min}, y_{max})	$[-0.07, 0.07]$ [m]
V_x, V_y, V_z	$[-0.12, 0.12]$ [m/s]

affect the spacecraft and may bring the chaser to collide with the target.

In [8], both classical and robust MPC (not TRMPC) have been adopted to solve the problem of RVD of spacecraft, using the HCW model where additive disturbances affect the system during the maneuver. The results show the classical MPC is not able to handle disturbances. Hence, in this section the simulation results related to the application of an LQMPC in the presence of persistent disturbances will not be reported. On the other hand, a different robust approach with respect to [8], i.e., TRMPC approach, has been implemented into a MATLAB/Simulink three DoF orbital simulator to show how the chosen controller is able to handle the persisting uncertainties due to the external environment and still robustly satisfy the mission and system constraints. In this Section, we briefly show the results related to the application of the TRMPC approach to the three DoF system translational dynamics. The system of the form of (2) is affected by persistent bounded disturbances, related to three main causes: (i) Earth-oblateness resulting in an asymmetric gravity potential J_2 term and a gravity gradient effect; (ii) drag due to the residual atmosphere; (iii) solar radiation pressure. The other environmental effects due to third-bodies or disturbances due to thrusters plum interactions are neglected because of the lower impact on the system. Hence, the set of additive disturbance considered is defined as $w \in \mathbb{W} = \left\{ w \mid ||w||_\infty \leq 10^{-2} \right\}$. The system is subject to hard constraints on both states and inputs. The uncertain sets have been introduced in Section 2. The cone geometry and the defining parameters are reported in Table 1, whereas the tightened constraints are reported in Table 2.

The Chaser vehicle is modeled as a cubic-shape spacecraft (1.2 m side) with a mass of 600 kg and equipped with six thrusters, two along each body axis and in two different orientation, each with a specific impulse of $I_{sp} = 220$ s and a maximum thrust of $F_{max} = 1$ N. The reference scenario sees the Chaser and the Target in a Low Earth Orbit with an altitude of 650 km, at an initial relative distance of -350 m along the V-bar axis. Moreover, the active vehicle has a residual velocity of 0.05 m/s with respect to the passive one.

The diagonal matrices $\mathbf{Q}$ and $\mathbf{R}$ are set to $10^2 \times \mathbb{I}_6$ and $\mathbb{I}_3$, respectively, while $\mathbf{P}$ is the solution of the discrete Algebraic Riccati equation. Furthermore, simulation settings are listed in Table 3.

To show the effectiveness of the TRMPC approach for the last phase of a space rendezvous maneuver, a set of simulations considering different Initial Conditions (ICs) within the entry cone have been performed considering a minus V-bar approach, in order to highlight the performance of the controller for each initial state vector within the state constraint set $\mathbb{X}$. Fig. 4 and Fig. 5 represent the 3D nominal and disturbed trajectories, respectively. We can see how the mission constraints in terms of position are satisfied, both within the cone in the orbital plane and the out-of-plane corridor. Each trajectory is driven to converge to the V-bar axis, according to a decreasing profile of the velocity along the approaching axis and satisfying the terminal constraints of null residual velocity between the spacecraft. Moreover, comparing the two figures, it is clear how the effect of disturbances is perceived strongly in the last part of the maneuver, but also in this phase, the proper definition of tightened constraints ensure the mission and system constraints satisfaction in the presence of additive disturbances, within the prescribed final safe region.

Table 3
3DoF MPC design parameters and model initialization settings.

Parameter	Value
MPC sample time	1 [s]
Prediction horizon	10
System sample time	1 [s]

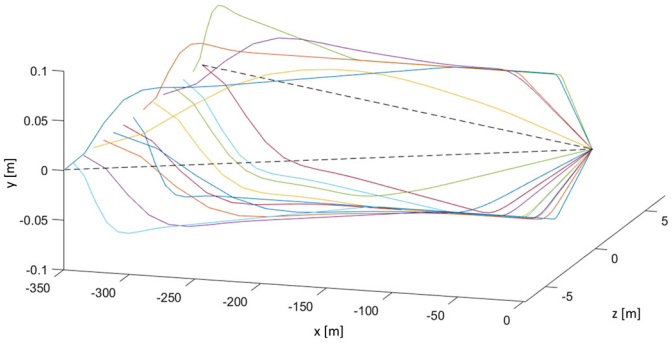

Fig. 4. TRMPC nominal simulated trajectories for different initial conditions.

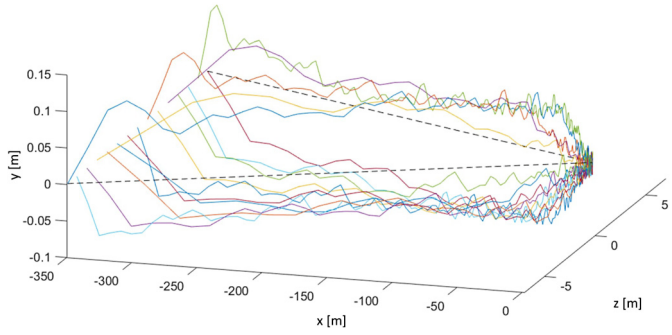

Fig. 5. TRMPC uncertain simulated trajectories for different initial conditions.

7. Experimental results

7.1. Scenario initialization

In this section, the results related to the application of TRMPC to the FSS system dynamics are here presented, together with the results obtained applying the LQMPC scheme to compare the performance of the two controllers in the presence of persistent disturbance. The experimental setup is composed by two FSSs, one moving representing the Chaser and the other one fixed, the Target, each one with a mass of 9.966 kg and equipped with a set of eight thrusters of 0.15 N on-board, controlled via a Sigma-Delta Modulation method [28]. First, the MATLAB/Simulink based numer-

Table 4
State and control constraints.

Parameter	Uncertain value	Nominal value
F_{max}	±0.15 [N]	±0.0927 [N]
ϕ	10 [deg]	8 [deg]
θ	$\pm 2\pi$ [rad]	±6.2496 [rad]
V_x, V_y	±0.2 [m/s]	±0.1777 [m/s]
$\dot{\theta}$	±0.1 [rad/s]	±0.0777 [rad/s]

Table 5
FSS MPC design parameters and model initialization settings.

Parameter	Value
MPC sample time	3 [s]
Prediction horizon	20
System sample time	0.01 [s]
GNC sample time	0.02 [s]
Maximum simulation time	450 [s]

ical simulator that recreates the whole FSS system, reproducing its dynamics and emulating the on-board sensors and actuators, is used to validate the models and tune the controllers. Then, the experiments are conducted on the NPS-POSEIDYN testbed [17]. The FSS has an on-board PC-104 computer based on an Intel Atom 1.6 GHz 32 bit processor with a 2 GB of RAM and an 8 GB solid-state drive. The operating system of the on-board computer is an RTAI-patched Ubuntu 14.04 Sever Edition which provides real-time execution capabilities. The developed LQMPC and TRMPC controllers are cross-compiled for the FSS 32-bit architecture and later transferred to the FSS.

The discrete-time linearized system is of the form (2), where the persistent disturbances affecting the system are defined as zero-mean random variables defined in an aforementioned convex and compact set $\mathrm{w} \in \mathbb{W} = 10^{-2}\mathbb{I}_6$.

The hard constraints on states and inputs are defined in Table 4 for the uncertain system, which represent also the constraints for the LQMPC setup, together with the tightened constraints defined for the TRMPC problem. The matrices $\mathbf{Q}$ and $\mathbf{R}$ are set to $diag(10^4\ 10^4\ 10^0\ 10^8\ 10^8\ 1)$ and $diag(10^6\ 10^6\ 9 \times 10^4)$, respectively, while $\mathbf{P}$ is the solution of the discrete Algebraic Riccati equation. Whereas, for what concerns the model initialization settings, they are resumed in Table 5 and have been adopted for both testbed simulations and experiments. Considering the computation time of the TRMPC algorithm and sample time, we adopt a prediction horizon of 20 in order to guarantee the stability of the system and be compliant with the testbed constraint of maximum computation time.

According to the mission scenario described in the previous Section, two different case studies have been selected, considering the following ICs:

1. Case A: (3.50 3.50 0 0 0 0), representing the optimal case from a mission point of view, since the large margin the Chaser has with respect to the cone boundaries,
2. Case B: (3.50 2.65 0 0 0 0), corresponding to the worst-case scenario, where the spacecraft is close enough to one of the cone limit that, in presence of uncertainty and without a proper control, it could easily violate the cone constraints.

Each case study has been experimentally reproduced several times, to validate the behavior of the controller. The result analysis is based on the following performance parameters:

Table 6
Performance of controllers in Case A (LQ = LQMPC, TR = TRMPC).

MPC method	Time to-dock [s]	Control effort [Ns]	Avg/Max iter. [–]	Dock Y/N
LQ (sim.)	450.00	4.16	8.95/10	N
TR (sim.)	450.00	11.81	8.91/9	Y
LQ (exp.)	329.04	6.77	8.65/9	N
TR (exp.)	337.90	17.47	9.47/10	Y

Table 7
Performance of controllers in Case B (LQ = LQMPC, TR = TRMPC).

MPC method	Time to-dock [s]	Control effort [Ns]	Avg/Max iter. [–]	Dock Y/N
LQ (sim.)	450.00	3.82	8.94/10	Y
TR (sim.)	450.00	11.60	8.90/9	Y
LQ (exp.)	301.13	5.22	8.58/9	Y
TR (exp.)	320.65	16.07	9.46/10	Y

- Time-to-dock, which defines the total duration of the maneuver performed by the Chaser to reach the Target, starting from the initial condition;
- Control effort, which measures the efficiency of the control approach and represents a fuel consumption estimation.

The controller performance in terms of computational time and control effort are reported in Table 6 for Case A, and Tables 7 for Case B. In addition, the satisfaction or violation of the constraints represents the third parameter in terms of how the optimization-based controller is able to handle the disturbances present in the system. Moreover, it is important to highlight that all the trajectories depicted in Figs. 6, 7 and 8 have been obtained with respect to a minimum-effort performance index. Indeed, while the rendezvous maneuver duration does not represent a stringent constraint, the control effort is linked to the fuel consumption as well as to the mission cost, hence it shall be minimized.

7.2. Case A

The trajectories obtained in Case A are represented in Fig. 6 for LQMPC and TRMPC, respectively. The first relevant difference is related to the divergence of the experimental trajectory with respect to the simulated one for the LQMPC approach. This behavior can bring the Chaser to not dock the Target at the end of the maneuver. In two over three experiments, the Chaser missed the Target, for the LQMPC approach, as shown in Fig. 6(a). On the other hand, the TRMPC approach shows a quasi-perfect match between the simulation and experiment (see Fig. 6(b), finalizing the trajectory with the docking. In this case, even if the data reported in Table 6 show that the robust approach is slower and more fuel-consuming, i.e., the control effort is more than double in the experimental environment, the main goal of the maneuver is to bring the Chaser to dock the Target, even in presence of persistent known disturbance. According to that, in this case the LQMPC approach cannot satisfy this objective when additive disturbance are acting on the system, since the drift action brings the spacecraft far from the terminal position of the Target.

7.3. Case B

Case B represents the most critical one, because of the vicinity to the cone boundary. In this case, the docking condition is reached for both the approaches. However, there are several differences between the results obtained for the two MPC methods, as represented in Fig. 7 and according to the controllers performance parameters in Tables 6 and 7. In the second scenario, the

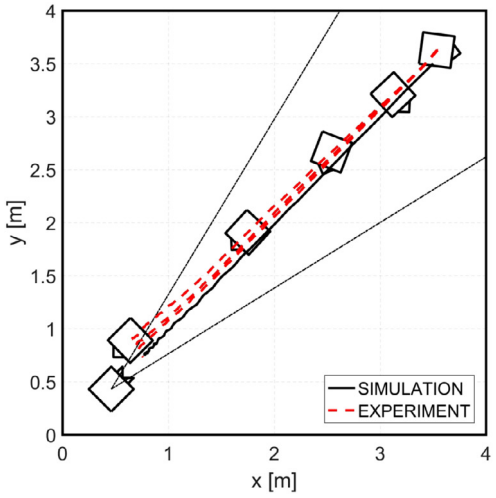

(a) LQMPC

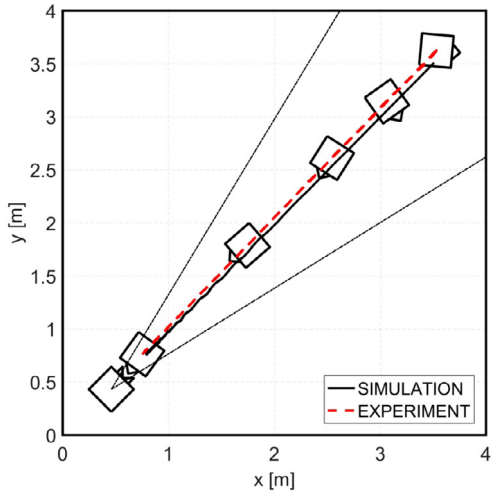

(b) TRMPC

Fig. 6. Comparison of simulation and experimental trajectories in Case A. Three different experimental results are represented for each approach. The Chaser is represented at time $t_0 = 0$ s, $t_1 = 20$ s, $t_2 = 100$ s, $t_3 = 200$ s.

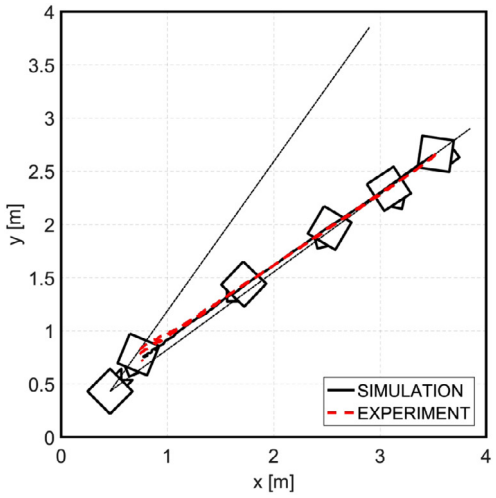

(a) LQMPC

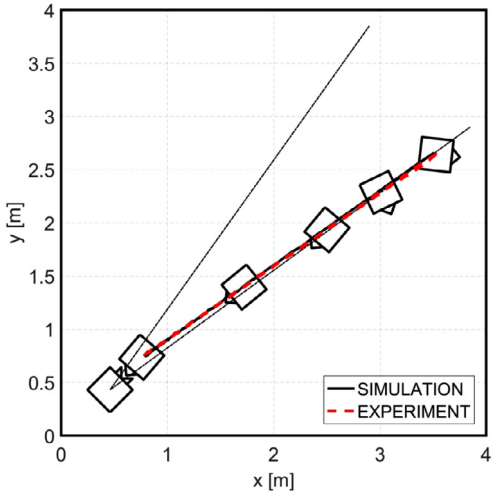

(b) TRMPC

Fig. 7. Comparison of simulation and experimental trajectories in Case B. Three different experimental results are represented for each approach. The Chaser is represented at time $t_0 = 0$ s, $t_1 = 20$ s, $t_2 = 100$ s, $t_3 = 200$ s.

LQMPC also allows a faster maneuver, even if the difference is significant only comparing the experimental results. Considering the control effort, the TRMPC proves itself to be the more fuel consuming approach, in the order of two/three times more. Nonetheless, in terms of constraint satisfaction, the robust approach validates its robustness to bounded additive disturbance (see Fig. 7(b)), whereas the classical approach cannot deal with the uncertainty properly, as shown in Fig. 7(a), specially in the last part of the maneuver, as highlighted in Fig. 8. In fact, in the latter case, the Chaser violates the cone boundary, failing the docking in the experimental set up (see Fig. 8(a)) and the required attitude is not well-achieved.

8. Conclusions

Considering the maneuver of rendezvous and docking (RVD) between two spacecraft as a mission scenario, the performance of two Model Predictive Control (MPC) schemes, one deterministic and one robust, have been compared in presence of persistent additive disturbance. A Tube-based Robust MPC (TRMPC), related to the approach already proposed in literature, has been adopted for the first time within this scenario as robust scheme, to guarantee robustness and suitable computational effort for real-time implementations. The stability of this robust scheme is ensured through a Linear Matrix Inequalities (LMI) approach, taking into account possible parametric uncertainty representing unmodeled dynamics, and neglected nonlinearities. Focusing on the robust approach, the Chaser spacecraft satisfies the hard state and control constraints and performs an autonomous docking with the Target, both in simulation (three degree-of-freedom (DoF) orbital simulator) and experimental environment (three DoF air-bearing testbed). On the other hand, the deterministic LQMPC is not always able to satisfy the state and input constraints, especially, in terms of cone boundaries, i.e., the Chaser cannot dock the Target. The results shown that they can be implemented on-board for the real-time control of the final phase of the RVD maneuver, with a comparable computational effort, even if the fuel consumption is higher when the robust approach is adopted. Hence, if the constraint satisfaction represents the main mission requirement, the TRMPC guarantees better performance.

In this work, V-bar approach has been chosen as capture axis, referring to the RVD mission profile of Soyuz, Progress and ATV vehicles. The effectiveness of the controller is ensured by the terminal cost, defined with respect to the reference final position to be reached and the control strategy is not tailored with respect

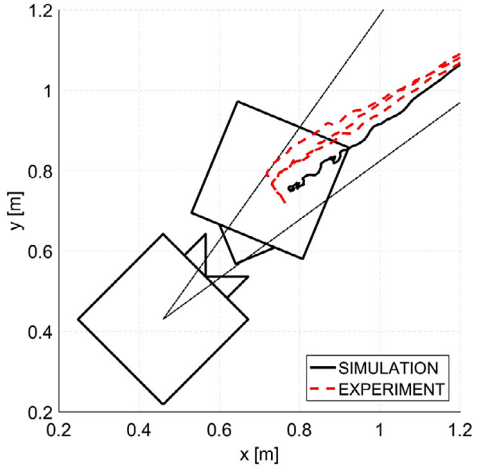

(a) LQMPC

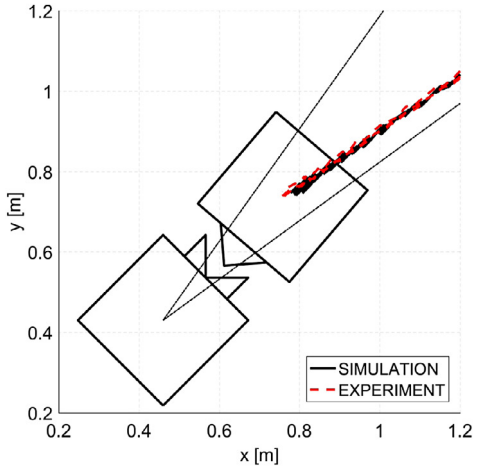

(b) TRMPC

Fig. 8. Zoomed-in trajectory of Case B for LQMPC and TRMPC. Three different experimental results are represented for each approach.

to the scenario considered, from a theoretical viewpoint. Finally, a tracking approach could be exploited, driving the error between the actual state and the desired one to zero. In this case, the TRMPC approach also remains valid and all the properties stand if the cost function as well as the state constraint set are re-defined with respect to the deviation $\delta x = x - x_{ref}$. Thanks to the flexibility of the proposed controller, it could be exploited also for different space scenarios such as: (a) R-bar approach, considering the mission profile of Soyuz and Progress vehicles on the nadir pointing side of the ISS Docking and Storage Module; (b) station-keeping; (c) attitude control, accounting for various mission objectives and type of spacecraft.

Conflict of interest statement

No conflict of interest.

Acknowledgements

The authors wish to thank Roberto Tempo and Fabrizio Dabbene, at CNR-IEIIT, Politecnico di Torino, and Matthias Lorentzen, at Institute for Systems Theory and Automatic Control of the University of Stuttgart, for their precious support provided for the theoretical definition of the TRMPC problem. The authors would also thank Josep Virgili-Llop and Costantinos Zagaris, at the Naval Postgraduate School, for the support in performing experiments.

References

[1] K. Subbarao, S. Welsh, Nonlinear control of motion synchronization for satellite proximity operations, J. Guid. Control Dyn. 31 (5) (2008) 1284–1294.
[2] D. Lee, J. Cochran Jr., T. No, Robust position and attitude control for spacecraft formation flying, J. Aerosp. Eng. 25 (3) (2012) 436–447.
[3] E. Capello, E. Punta, F. Dabbene, G. Guglieri, R. Tempo, Sliding mode control strategies for rendezvous and docking maneuvers, J. Guid. Control Dyn. 40 (6) (2017) 1481–1487.
[4] Y. Luo, J. Zhang, G. Tang, Survey of orbital dynamics and control of space rendezvous, Chin. J. Aeronaut. 27 (1) (2014) 1–11.
[5] T. Rybus, K. Seweryn, Planar air-bearing microgravity simulators: review of applications, existing solutions and design parameters, Acta Astronaut. 120 (2016) 239–259.
[6] S. Di Cairano, H. Park, I. Kolmanovsky, Model predictive control approach for guidance of spacecraft rendezvous and proximity maneuvering, Int. J. Robust Nonlinear Control 22 (12) (2012) 1398–1427.
[7] M. Leomanni, E. Rogers, S.B. Gabriel, Explicit model predictive control approach for low-thrust spacecraft proximity operations, J. Guid. Control Dyn. 37 (6) (2014) 1780–1790.
[8] F. Gavilan, R. Vazquez, E.F. Camacho, Robust model predictive control for spacecraft rendezvous with online prediction of disturbance bounds, 2011.
[9] B. Kouvaritakis, M. Cannon, Model Predictive Control: Classical, Robust and Stochastic, Advanced Textbooks in Control and Signal Processing, Springer, 2015.
[10] K. Graichen, B. Kapernick, A real-time gradient method for nonlinear model predictive control, in: Tao Zheng (Ed.), Frontiers of Model Predictive Control, 2012.
[11] D.Q. Mayne, J.B. Rawlings, Model Predictive Control: Theory and Design, Nob Hill Publishing, LCC, Madison, WI, 2009.
[12] E. Granado, W. Colmenares, J. Bernussou, G. Garcia, Linear matrix inequality based model predictive controller, IEEE Proc. Control Theory Appl. 50 (5) (2003).
[13] Y. Fu, C. Li, Parametric method for spacecraft trajectory tracking control problem with stochastic thruster fault, IET Control Theory Appl. 10 (17) (2016) 2331–2338.
[14] W.H. Clohessy, R.S. Wiltshire, Terminal guidance system for satellite rendezvous, J. Aerosp. Sci. 27 (9) (1960) 653–658.
[15] J. Virgili-Llop, C. Zagaris, H. Park, R. Zappulla II, M. Romano, Experimental evaluation of model predictive control and inverse dynamics control for spacecraft proximity and docking maneuvers, CEAS Space J. 10 (1) (2018) 37–49.
[16] B.R. Barmish, New Tools for Robustness of Linear Systems, Macmillan Publishing Company, New York, 1994.
[17] R. Zappulla II, J. Virgili-Llop, C. Zagaris, H. Park, M. Romano, Dynamic air-bearing hardware-in-the-loop testbed to experimentally evaluate autonomous spacecraft proximity maneuvers, J. Spacecr. Rockets 54 (4) (2017) 825–839.
[18] W. Fehse, Automated Rendezvous and Docking of Spacecraft, vol. 16, Cambridge University Press, 2003.
[19] M. Dentis, E. Capello, G. Guglieri, A novel concept for guidance and control of spacecraft orbital maneuvers, Int. J. Aerosp. Eng. 2016 (2016) 7695257, https://doi.org/10.1155/2016/7695257.
[20] C. Lugini, M. Romano, A ballistic-pendulum test stand to characterize small cold-gas thruster nozzles, Acta Astronaut. 64 (2009) 615–625.
[21] A.C. Bartlett, C.V. Hollot, L. Huang, Root locations of an entire polytope of polynomials: it suffices to check the edges, Math. Control Signals Syst. 1 (1988) 61–71.
[22] R. Tempo, G. Calafiore, F. Dabbene, Randomized Algorithms for Analysis and Control Uncertain Systems, Springer Science & Business Media, 2012.
[23] L. Chisci, J.A. Rossiter, G. Zappa, Systems with persistent disturbances: predictive control with restricted constraints, Automatica 37 (7) (2001) 1019–1028.
[24] M. Lorenzen, F. Dabbene, R. Tempo, F. Allgöwer, Constraint-tightening and stability in stochastic model predictive control, IEEE Trans. Autom. Control 62 (7) (2017) 3165–3177.
[25] S.V. Rakovic, E.C. Kerrigan, K. Kouramas, D.Q. Mayne, Approximation of the minimal robustly positively invariant set for discrete-time LTI systems with persistent state disturbances, in: 42nd IEEE Conference on Decision and Control, Maui, Hawaii, 2003.
[26] M. Saponara, V. Barrena, A. Bemporad, E.N. Hartley, J. Maciejowski, A. Richards, A. Tramutola, P. Trodden, Model predictive control application to spacecraft rendezvous in Mars sample & return scenario, in: Proceeding of 4th European Conference for Aerospace Sciences, Saint Petersburg, Russia, 2011.
[27] P. Bodin, R. Noteborn, R. Larsson, C. Chasset, System test results from the GNC experiments on the PRISMA in-orbit test bed, Acta Astronaut. 68 (7) (2011) 862–872.
[28] R. Zappulla, J. Virgili-Llop, M. Romano, Spacecraft thruster control via Sigma-Delta modulation, J. Guid. Control Dyn. 40 (11) (2017) 2928–2933.